Autoconfocal microscopy with a cw laser and thermionic detection

Daryl Lim, Kengyeh K. Chu, and Jerome Mertz*

Department of Biomedical Engineering, Boston University, 44 Cummington Street, Boston, Massachusetts 02215, USA
**Corresponding author: jmertz@bu.edu*

Received February 27, 2008; revised May 3, 2008; accepted May 11, 2008; posted May 15, 2008 (Doc. ID 93225); published June 12, 2008

We introduce an application of thermionic emission in a PMT photocathode. Because of the nonlinear dependence of thermionic emission on absorbed laser power, a conventional PMT is found to produce a virtual pinhole effect that rejects unfocused light at least as strongly as a physical pinhole. This virtual pinhole effect is exploited in a scanning transmission confocal microscope equipped with a cw laser source. Because the area of the PMT photocathode is large, signal descanning is not required and thermionic detection acts as a self-aligned pinhole. Our technique of thermionic-detection autoconfocal microscopy is further implemented with graded-field contrast to obtain enhanced phase-gradient sensitivity in unlabeled samples, such as rat hippocampal brain slices.

OCIS codes: 180.0180, 180.1790, 180.5810, 190.4870.

Confocal laser scanning microscopy is a ubiquitous imaging modality that provides 3D resolution. This ability to resolve in 3D is afforded by the use of a pinhole, which rejects light that is not well focused and hence eliminates out-of-focus background. In particular, the power of light allowed through a pinhole is dependent on the power density (intensity) of the light incident on the pinhole, resulting in an inverse proportional relationship between detected power and incident beam area [1]. More generally, it should be noted that any detection process that is sensitive to power density rather than power leads to a similar relationship. For example, if the pinhole in front of a detector is replaced with a frequency-doubling crystal, then the resultant second-harmonic generation (SHG) power also scales inversely with the incident beam area. In this manner, a frequency-doubling crystal can act as a virtual pinhole, an effect that was recently exploited in the development of a self-aligned transmission confocal microscope called an autoconfocal microscope (ACM) [2,3]. Because SHG generally requires the use of pulsed illumination to provide adequate signal, an ACM based on SHG detection is primarily designed to be used in conjunction with two-photon excitation microscopy [4]. In this Letter, we describe an alternative strategy for nonlinear detection that does away with the need for pulsed illumination. Our new strategy employs thermionic emission, which is more conventionally treated as a source of noise. We demonstrate that the use of thermionic emission as a detection mechanism, i.e., thermionic detection (TD), leads to a virtual pinhole effect that can actually outperform a physical pinhole in terms of out-of-focus background rejection. Because TD can be operated with a simple cw laser, it can be integrated in any laser scanning microscope at low cost. In particular, we demonstrate the effectiveness of TD-ACM for phase-contrast imaging of brain tissue.

In practice, TD can be achieved with a conventional photomultiplier tube (PMT). If the frequency of the laser is chosen such that the energy of each incident photon is below the photoelectric work function of the PMT photocathode, then essentially no electrons are ejected via the photoelectric effect. However, photons absorbed by the photocathode nevertheless deposit heat. This heat can lead to an evaporation of electrons from photocathode surface, referred to as thermionic emission. In particular, if the system is in thermal equilibrium, then the temperature (T) of the photocathode becomes proportional to the power of the incident light. Thermionic emission flux (J) is then described by the well-known Richardson equation [5]

$$J = AT^2 \exp(-W_{eff}/k_B T), \tag{1}$$

where A is the Richardson constant, k_B is the Boltzmann constant, and W_{eff} is the effective work function of the PMT photocathode. In practice, W_{eff} is adjusted by applying an electric field at the photocathode (Schottky effect [6]), which can be accomplished by adjusting the PMT gain. In addition, W_{eff} can be boosted artificially by requiring the thermionic flux to exceed a user-defined energy threshold. We applied such a thresholding technique either electronically by a peak counting circuit at the PMT anode, or numerically by postprocessing the raw signal from the PMT.

To demonstrate thermionic detection, we illuminated a bialkali PMT (Hamamatsu HC-125-02) with a cw laser beam at 1064 nm (Roithner LaserTechnik DPSSL) focused to a spot size of about 10 μm. The photon energy corresponding to the laser-beam wavelength is far below the photoelectric work function of the PMT photocathode, meaning that any PMT output in this case arises primarily from thermionic emission [5]. The output of the PMT is then analyzed by a peak-counting algorithm. In all cases, the laser power is kept low enough so that each peak can be assumed to represent the ejection of a single electron from the photocathode. The number of peaks counted

thus gives a measure of J, which we fit to Eq. (1) by plotting against laser power (Fig. 1). The strength of the fit ($R^2=0.998$) is strong evidence that thermionic emission was responsible for the generation of electrons from the photocathode. In addition to counting peaks, we also integrated the output of the PMT to obtain the mean output (Fig. 1). The resulting curve is also nonlinear, indicating that taking the mean as the output of TD would also result in a virtual pinhole effect. The relationship appears to be quadratic in nature ($R^2=0.995$), the source of which we believe is again the Richardson equation, but with W_{eff} significantly reduced because we have omitted thresholding. By contrast, a linear curve would be expected if the electrons were instead generated by the photoelectric effect.

We expanded the above experiment to modulate the laser power with an electro-optic modulator (EOM) in order to determine the bandwidth of the detection system. With no modulation, the detector output remained constant, indicating that our assumption that the photocathode achieves thermal equilibrium is valid. Indeed, the detection bandwidth was found to exceed 1 MHz (the bandwidth of our EOM), indicating that thermal equilibrium is attained quite rapidly.

The advantage of a virtual pinhole over a physical pinhole lies in the size of the detector. This advantage is especially significant in the transmission case, since the scanned output light is not naturally descanned by the scanning illumination optics into a fixed-location pinhole [2]. In a TD-ACM, a virtual pinhole effect is exhibited over the entire surface of the PMT photocathode, eliminating any need for descanning. This advantage allows TD-ACM to be easily implemented in a transmission configuration, as illustrated in Fig. 2.

To confirm the capacity of TD to produce a virtual pinhole effect, we first operated our TD-ACM in the absence of a sample, with no scanning, and with only moderate focusing at the photocathode (beam waist ~ 10 μm). We then axially translated the photocathode through the focal plane ($z=0$). Even though the total incident laser power at any z plane is a constant, PMT output is not constant, since thermionic emission has a nonlinear dependence on temperature, and hence absorbed power. The result is that PMT output increases with intensity and is maximized where the beam is most focused (Fig. 3). The PMT output is then handled in two separate ways: counting the number of peaks, or integrated to find the mean of the output. The FWHM of each curve is thus a measure of the unfocused-light rejection capability of the respective technique. As expected from the results shown in Fig. 1, the curve produced by counting peaks has a narrower FWHM (480 μm) than that obtained by taking the mean (910 μm). A linear detector, more specifically a photodiode (Thorlabs DET110), equipped with a physical pinhole (10 μm diameter), produces a curve similar to that obtained by taking the mean TD output, suggesting that integrating the TD output would provide approximately the same pinhole effect as a physical pinhole.

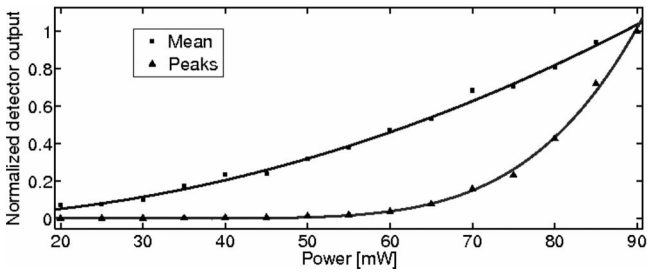

Fig. 1. A laser beam (1064 nm) is focused onto a bialkali PMT photocathode to generate thermionic emission. Peak counts (triangles) or the mean of the output (squares) are plotted against laser power. Solid curves indicate fits to the Richardson equation and to a quadratic, respectively.

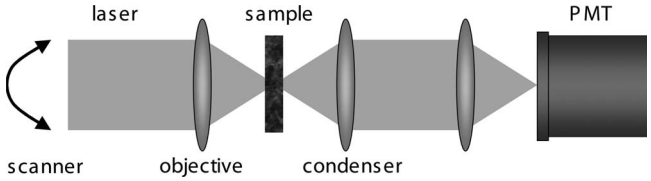

Fig. 2. TD-ACM schematic. A focused laser beam is scanned across a sample. Light transmitted through the sample is collected and focused onto the photocathode of a PMT. The resulting thermionic current is amplified by the PMT and then fed into a peak counting circuit to obtain J, or integrated to obtain the mean.

Finally, having demonstrated the capability of TD to produce a virtual pinhole effect, we applied TD-ACM to imaging a biological sample, in this case a 400-μm-thick tissue slice from a rat hippocampus. In addition to the laser and PMT specified previously, our setup includes an Olympus 20× water-immersion objective with a numerical aperture of 0.95 to focus the laser beam into the tissue. The output of the PMT is taken as the pixel value and provides a measure of the local extinction in the sample. While the implementation of the peak counting circuit is expected to enhance the virtual pinhole effect, we found that in practice it led to an increase in noise in the system without significantly improving image quality. Our results are therefore presented using PMT signal integration rather than peak counting.

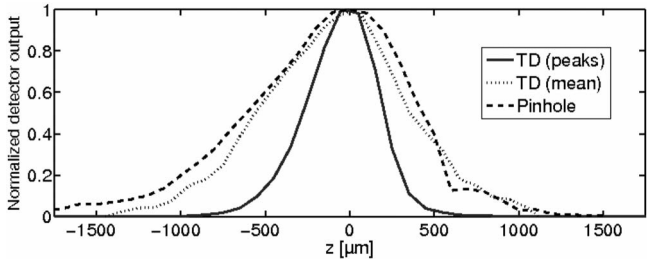

Fig. 3. Virtual pinhole effect. Unfocused-light rejection capability of TD is demonstrated by sliding the PMT along z through the focal plane ($z=0$) of a focused beam of confocal parameter about 1 mm. The output of the PMT is either integrated to find the mean (dotted curve), or analyzed by a peak counting algorithm (solid cuve) to find J. The FWHM of the curve obtained by integrating is roughly the same as that obtained using a photodiode equipped with a physical pinhole (10 μm diameter). The FWHM obtained by peak counting is significantly narrower.

Because a brain slice exhibits little absorption contrast, we equipped our TD-ACM with graded-field contrast [3] so as to obtain phase-gradient sensitivity. In brief, graded-field contrast consists of introducing partial beam blocks into the Fourier planes both before and after the sample, such that most of the ballistic light is blocked. Depending on the orientation of a phase gradient in the sample, light scattered from the phase gradient becomes more or less obstructed by the downstream beam block. Thus phase gradients in the sample are converted into power variations of the detected light, leading to phase gradient sensitivity similar to that obtained with differential interference contrast microscopy.

To illustrate the unfocused-light rejection capability of TD-ACM, we compare an image taken with TD-ACM [Fig. 4(a)] to one taken with a linear detector, i.e. a photodiode with no pinhole [Fig. 4(b)]. The graded-field technique was applied in both cases to provide phase-gradient contrast. While pyramidal neurons are visible in both images, the unfocused-light rejection capability of TD-ACM results in much higher contrast and reveals subtle features in the rat hippocampus not apparent in the image taken by the linear detector. By rejecting background scattered light, TD-ACM is capable of imaging deep (>150 μm) into the scattering brain tissue while maintaining high contrast [Figs. 4(c)–4(e)]. No streaking is observed in the TD-ACM image, which confirms that thermal equilibrium is reached quickly enough in the photocathode to image at our pixel scan rate of 125 kHz. It should be noted that TD-ACM requires a fairly uniform response across the photocathode surface (in our case, about 4 mm^2), which is largely ensured here because our PMT is meshless.

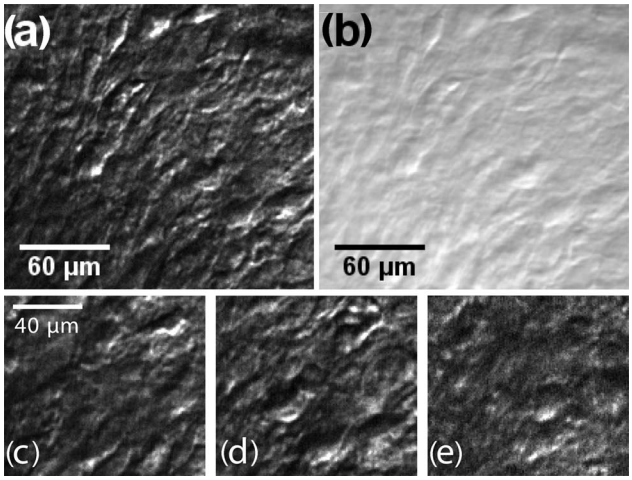

Fig. 4. Graded-field-contrast-enhanced image of a rat hippocampus slice (400 μm thick) acquired with (a) TD-ACM and (b) a linear detector. Both images were acquired 70 μm below the tissue surface. (c)–(e), TD-ACM images of same sample taken at depths 30, 60 and 150 μm. Acquisition time was 2.8 s with an illumination power incident on the sample of about 25 mW. All images were subjected to $4\times$ averaging and a gamma of 0.75. Panels (a) and (b) are 380×350 pixels.

A drawback of TD-ACM is that it is based on the Richardson equation, which is critically dependent on W_{eff}. Since W_{eff} is generally not known *a priori*, the images generated by TD-ACM are uncalibrated. However, a straightforward approach to calibrating the images could be through the use of adaptive illumination (AI) [7]. AI refers to the use of an active feedback system that sets the PMT output to a user-defined set point by rapidly adjusting the illumination power. Since the AI image reconstruction algorithm is essentially independent of the Richardson equation, a calibrated image can then be obtained by simply inverting the output of the feedback signal, i.e., the illumination power (see [7] for details).

In conclusion, we have introduced a novel application of thermionic emission in a transmission autoconfocal microscope. By exploiting the process of thermionic emission, we obviate the need for a pulsed laser, which is required for SHG-ACM. Besides being self-aligning, the virtual pinhole effect provided by TD is found to reject out-of-focus background light at least as strongly as a physical pinhole. Our results are corroborated by images of a rat brain slice, enhanced by graded-field contrast, which demonstrate the deep tissue imaging capability of a TD-ACM. Since the laser source need only be cw, TD-ACM can be easily integrated with a standard fluorescence confocal microscope. The TD-ACM add-on would consist only of basic lenses and a suitable laser-PMT pair.

References

1. T. Wilson and C. J. R. Sheppard, *Theory and Practice of Scanning Optical Microscopy* (Academic, 1984).
2. T. Pons and J. Mertz, J. Opt. Soc. Am. B **21**, 1486 (2004).
3. K. K. Chu, R. Yi, and J. Mertz, Opt. Express **15**, 2476 (2007).
4. W. Denk, J. H. Strickler, and W. W. Webb, Science **248**, 73 (1990).
5. P. B. Coates, J. Phys. D **5**, 1489 (1972).
6. W. Schottky, Annalen der Physik **362**, 541 (1918).
7. K. K. Chu, D. Lim, and J. Mertz, Opt. Lett. **32**, 2846 (2007).